Both cell-intrinsic and environmental factors constrain speed and persistence in T cell migration

Inge M N Wortel [1,*], Ioana Niculescu [2], Martijn Kolijn [2], Nir Gov [3], Rob J de Boer [2], and Johannes Textor [1,2]

June 4, 2018

[1]Department of Tumor Immunology, Radboud Institute for Molecular Life Sciences, Nijmegen, the Netherlands
[2]Theoretical Biology and Bioinformatics, Department of Biology, Utrecht University, Utrecht, the Netherlands
[3]Department of Chemical and Biological Physics, Weizmann Institute of Science, Rehovot, Israel

Abstract

T cells are key effector cells in the immune system that are well-known for their ability to adapt their shape and behavior to environmental cues. It has been suggested that these highly diverse, context-dependent migration patterns reflect an optimization process – where T cells adjust motility parameters such as speed and persistence to aid their search for antigen. Whereas models investigating such "search strategies" typically treat speed and persistence as independent variables, one aspect of cell motility was recently found to be conserved across a large variety of cell types: fast-moving cells turn less frequently. This raises the question whether T cells can tune speed and persistence independently of each other. We therefore investigated to what extent this universal coupling between cell speed and persistence (UCSP) shapes the behavior of migrating T cells. We first show that the UCSP emerges spontaneously in an *in silico* Cellular Potts Model (CPM) of T cell migration. Our model shows a link between the UCSP and cell shape dynamics, which put an upper bound on both the speed and the persistence a cell can reach. We then use the CPM to examine how environmental constraints affect motility patterns of T cells migrating in the crowded environments they also face *in vivo*, and show that T cells completely lose their speed-persistence coupling when confined in a densely packed environment such as the epidermis. Thus, although our model further highlights the validity of the UCSP in migrating cells, it also demonstrates that environmental factors may overrule this coupling. Our data show that T cell motility parameters are subject to both cell-intrinsic and extrinsic constraints, suggesting that "optimal" T cell search strategies may not always be attainable *in vivo*.

Keywords: T cell migration, Directed migration, Universal Coupling Speed and Persistence (UCSP), Cellular Potts Model, T cell search strategies

1 Introduction

T cells have the rare ability to migrate in nearly all tissues within the human body. Especially in tissues with a high risk of infection – like the lung, the gut, and the skin – T cells are continuously on the move in search of foreign invaders. Furthermore, migration in lymphoid organs such as the thymus and lymph nodes is crucial for T cell function.

Although T cells preserve their motility in these different contexts, they do adapt their morphology and migratory behavior to environmental cues. It has been suggested that this remarkably flexible behavior reflects different "search strategies" that allow T cells to maximize the chance of encountering antigen (Krummel et al., 2016). For example, naive T cells rapidly crawl along a network of stromal cells in the lymph node, alternating between short intervals of persistent movement and random changes in direction (Miller et al., 2002, 2003; Bajnoff et al., 2006; Beauchemin et al., 2007). This "stop and go" behavior allows them to cover large areas of the lymph node in a short amount of time, and appears to be a good strategy for finding rare antigens without prior information on their location (Krummel et al., 2016; Bnichou et al., 2011; Tejedor et al., 2012; Chupeau et al., 2015). Developing T cells adopt a similar strategy to find their specific ligand during negative selection in the thymic medulla (Borgne et al., 2009; Klein, 2009). By contrast, positive selection in the thymic cortex involves migration at much lower speeds – which is thought to reflect the more broad distribution of positively selecting ligands in the thymus (Germain et al., 2012). Thus, different migration strategies may be optimal in different environments and contexts.

Studies investigating these T cell search strategies typically rely on variations of random walk models (Krummel et al., 2016). Such models assume that T cells can tune motility parameters (such as speed and turning behavior) independently of each other to obtain an "optimal" movement pattern. However, recent data suggest that this may not be the case, because a Universal Coupling between Speed and Persistence (UCSP) appears to exists in all migrating cells (Maiuri et al., 2012; Wu et al., 2014; Maiuri et al., 2015). Among cell tracks recorded under standardized conditions, Maiuri et al saw that all cells analyzed followed one general rule: faster cells moved more persistently. They proposed that this coupling arises from a positive feedback on cell polarity regulated by movement of the actin cytoskeleton. Because specialized clutch molecules keep actin filaments fixed with respect to the cell's surroundings, these filaments move backwards in the reference frame of the moving cell. This "actin retrograde flow" is linearly dependent on cell speed. Using a mathematical model, Maiuri et al were able to show that actin retrograde flow can also stabilize cell polarity (and thus persistence) if it transports polarity cues towards the cell's rear end. Thus, higher speeds are linked to higher persistence because they stabilize cell polarity via the actin retrograde flow (Maiuri et al., 2015). As actin retrograde flow is a highly conserved feature of cell migration, the UCSP is a general migration law that holds for celltypes with very different migration modes.

Maiuri et al derived the UCSP from experiments where cells moved freely in a relatively open space, without any of the barriers normally posed by surrounding tissue. However, T cells rarely move in open space, and *in vivo* imaging as well as *in silico* modelling studies have highlighted the importance of external cues for T cell migratory behavior (Bajnoff et al., 2006; Beltman et al., 2007). A key open question is therefore whether the UCSP remains the major determinant of speed and persistence for T cells migrating in such complex, crowded environments – making the UCSP a truly universal law of T cell migration *in vivo*.

Here, we examine to what extent the UCSP can impact T cell migration patterns, using an existing Cellular Potts Model (CPM) of T cell migration that reproduces realistic cell shapes and migratory behavior *in silico* (Niculescu et al., 2015). We first show that this model not only reproduces the UCSP, but also explains how cell shape dynamics put a natural upper bound on both the speed and persistence of migrating cells. We then apply the CPM to the extreme case of T cell migration in a densely packed epidermis, and show that environmental constraints overrule the UCSP in this setting. Thus, our data confirm the universality of the UCSP across a range of different cell shapes and migration modes, but also predict that this cell-intrinsic coupling may be obscured in at least some of the environments T cells face *in vivo* – where cell-extrinsic factors place more stringent constraints on motility parameters.

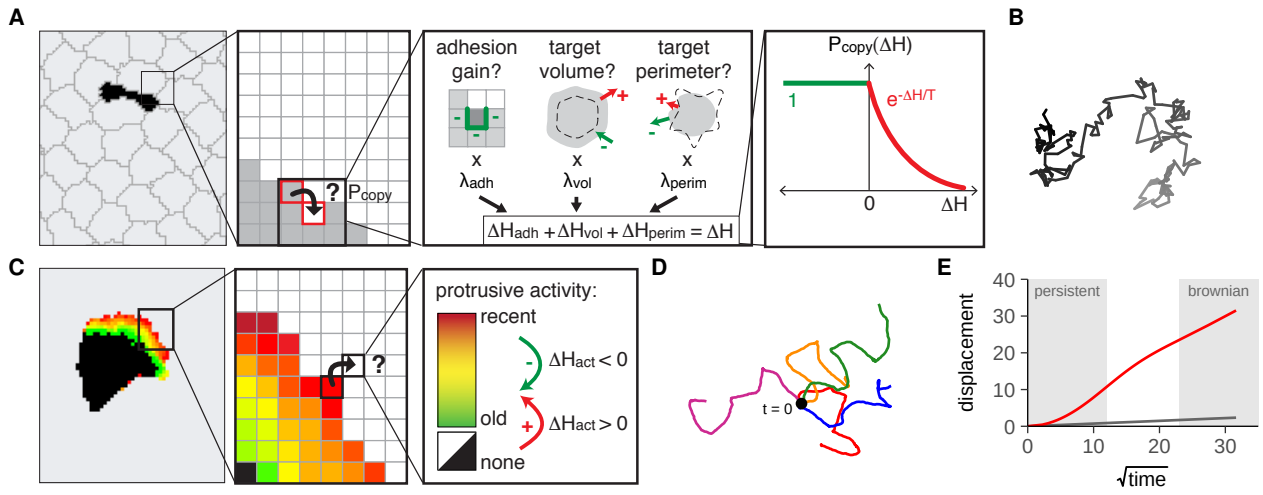

Figure 1: *In silico* simulation of shape-driven T cell migration within complex environments. **(A)** A CPM models a tissue as a collection of pixels on a grid that each belong to a specific cell (or to surroundings). Pixels randomly try to copy their cell identity into pixels belonging to neighbor cells, with a success probability P_{copy} that depends on the effect the change would have on physical properties of the involved cells (cell-cell adhesion, and deviation from target volume/perimeter, dashed lines). The weighted sum of these energetic effects (ΔH) is negative when a copy attempt is energetically favourable. **(B)** In a CPM with only adhesion, volume, and perimeter constraints, cells only exhibit Brownian motion. Plot shows an example cell track. **(C)** In the Act model (Niculescu et al., 2015), each pixel has an "activity" that represents the time since its most recent protrusive activity. Copy attempts from active to less active pixels are stimulated (negative ΔH_{act}), whereas copy attempts from inactive to more active pixels are punished (positive ΔH_{act}). **(D)** Act cells alternate between persistent motion and "stops" in which they change direction. Plot shows example tracks of 5 Act cells with overlaying starting point (black dot, t = 0). **(E)** Displacement plot of CPM cells simulated with and without the Act extension. Brownian motion (without the Act model, gray line) results in a linear curve. Act cell movement appears as brownian motion on large time scales (linear part of red line), but is persistent on smaller time scales (non-linear start of red line).

2 Results

2.1 An extended Cellular Potts Model reproduces features of T cell migration

To investigate how external cues affect the cell-intrinsic coupling between speed and persistence in migrating T cells, we need a model that not only reproduces this coupling, but can also simulate realistic cell migration within the complex environments relevant to T cell biology. Such a model must provide a spatial description of the cell's shape and interaction with its surroundings – both of which are crucial for T cell behavior *in vivo* (Beltman et al., 2007; Ariotti et al., 2012). We therefore turned to a Cellular Potts Model (CPM). CPMs represent cells as collections of pixels that move by randomly trying to add or remove pixels at their borders ("copy attempts"). While doing so, cells try to minimize the energetic cost ΔH associated with maintaining their shape and contacts with neighbor cells (Figure 1A). This allows CPMs to reproduce realistic, dynamic cell shapes and -behavior using only a few simple rules and parameters. Their spatially explicit yet simple nature makes CPMs powerful tools for modelling the interactions of individual cells with complex, multicellular environments in a controlled setting. However, the energy that basic CPM cells try to minimize is based solely on adhesion and cell shape. As there is no energetic benefit for consistent movement in any given direction, these cells undergo brownian motion rather than migrating actively (Figure 1B).

We therefore use an extension of the CPM that does allow for active migration (Niculescu et al., 2015). In this "Act-model", pixels newly added to a cell temporarily remember their recent protrusive activity. Copy attempts from active into less active pixels are rewarded via a negative contribution ΔH_{act} to the cost ΔH, inducing a positive feedback loop wherein recently added pixels become more likely to protrude again (Figure 1C). Consequently, local groups of active pixels form stable protrusions that drag the cell forward in persistent motion before disappearing again, at which point the cell stops until a new protrusion forms. Thus, cells alternate between intervals of persistent movement and "stops", in which they can switch direction (Figure

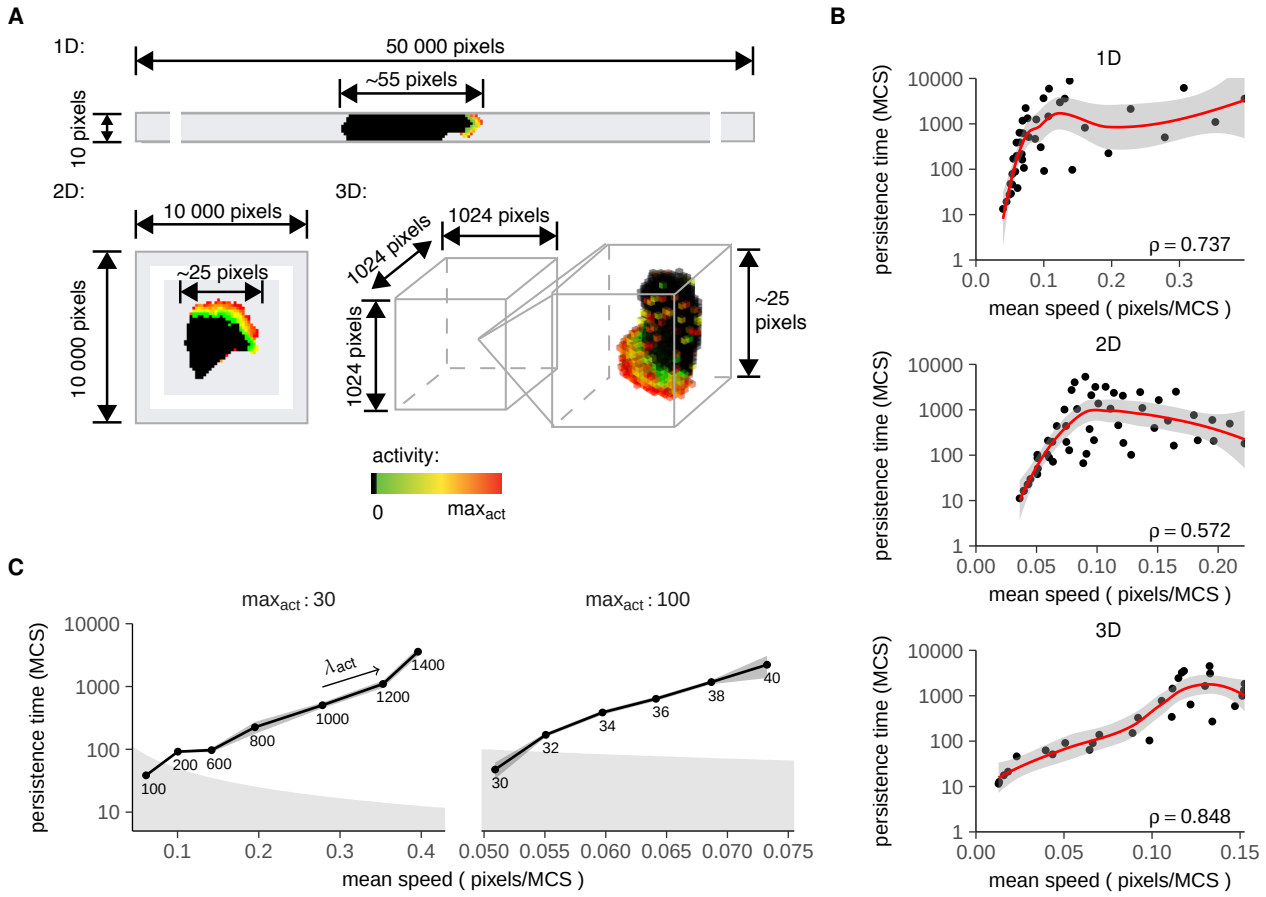

Figure 2: The Act model reproduces the UCSP observed in experimental data. **(A)** Set-up and example Act cells for simulations of 1D, 2D, and 3D migration. Color gradients indicate the active protrusion. Simulated microchannels ("1D" migration) consist of two parallel walls, leaving 10 pixels in between. 2D and 3D simulations were performed in an empty grid of the indicated sizes, with no external constraints on the cell shape. **(B)** Speed-persistence coupling arises in the Act model on an exponential scale. Plots show data from 1D, 2D, and 3D simulations, respectively (ρ = spearman correlation coefficient). See Materials and Methods for a list of parameters used. **(C)** Speed-persistence coupling is stronger for cells stratified by max_{act}. Plot shows mean ± SD of persistence time plotted against speed for Act cells migrating in microchannels (1D), grouped by value of max_{act}; numbers in the plot indicate the corresponding value of λ_{act}. Shaded gray areas in the background indicate regions where the persistence time is lower than the time it takes for the cell to move 10% of its length.

1D). At larger time scales, movement still resembles brownian motion (new protrusions can form in random directions). Persistence is only evident at the smaller time scales during which the cell has a stable protrusion and maintains its direction of movement (Figure 1E).

This behavior qualitatively resembles the characteristic "stop-and-go" motility of T cells searching for antigen in the lymph node (Miller et al., 2002; Beauchemin et al., 2007). Because the Act model can also simulate cell migration within tissues (Niculescu et al., 2015), this makes it a suitable tool for modelling the effect of tissue context on T cell migration dynamics *in silico*.

2.2 The Act model reproduces the UCSP observed in migrating cells

After showing that the Act model can reproduce several relevant features of T cell migration, we first tested whether it could also reproduce the UCSP observed in experimental data. Most of these experiments involved the migration of cells moving along adhesive tracks or within microchannels (Maiuri et al., 2012, 2015). To mimic this "one-dimensional" experimental set-up *in silico*, we constrained Act cells between two parallel walls, leaving a space of 10 pixels within the channel (Figure 2A). This set-up resulted in cell elongation comparable to that observed for cells moving on 1D adhesive tracks (compare Figure 2A to Figure 1B in (Maiuri et al., 2015)). Act cells moving in these microchannels display "stop-and-go" behavior, migrating persistently in one direction

until they lose their active protrusion – at which point they wait ("stop") for a new protrusion to form and can switch direction (Figure S1A in Supplementary Material).

In addition, Maiuri et al also observed the UCSP for cells migrating on surfaces ("2D") or within 3D environments (Maiuri et al., 2015). We mimicked these experiments by simulating Act cell migration on large 2D and 3D grids without microchannel walls (Figure 2A). In contrast to the uniform, elongated shape observed in channels, Act cells moving in 2D and 3D form protrusions of different shapes (Niculescu et al., 2015) (Figure 2A and see below).

We then used these different set-ups to simulate cells with different migratory behavior. Two parameters control migration in the Act model. The first, λ_{act}, tunes the contribution of the positive feedback ΔH_{act} relative to the other energetic constraints (adhesion, volume, perimeter), and can be interpreted as the force exerted on the cell membrane by actin polymerization in the cell's leading edge. When λ_{act} is large, this force can easily push the membrane forward to form a stable protrusion, but when it is small, the actin cytoskeleton has a hard time overcoming other, opposing forces (such as membrane tension). Higher λ_{act} values therefore yield larger protrusions (Figure S1B in Supplementary Material). The second parameter, max_{act}, determines how long pixels remember their activity (measured in MCS, the time unit of the CPM). It thereby puts an upper bound on the protrusion size, and can be interpreted as the lifetime of polymerized actin. Higher max_{act} values therefore have a stabilizing effect on the protrusions – yielding larger protrusions even at small forces λ_{act} (Figure S1B in Supplementary Material).

To simulate cells with variable migratory behavior, we generated cell tracks for Act cells with different λ_{act} and max_{act} values. Analysis of speed and persistence time (computed from the speed autocorrelation function, see Materials and Methods) revealed a weak exponential coupling between speed and persistence in all three settings (Figure 2B). Although the correlation was weak in these heterogeneous datasets of Act cells with highly different λ_{act} and max_{act} parameters, it became much stronger when we stratified cells by max_{act} value (Figure 2C). Analysis of speed and persistence in these tracks yielded the same exponential correlation between speed and persistence that was also observed in experimental data (Maiuri et al., 2015). This finding was independent of the choice of max_{act}, as we found similar curves for different values of max_{act} (Figure 2C). These results demonstrate the existence of a speed-persistence coupling in the Act model.

2.3 Speed-persistence coupling in the Act model spans a range of migration modes

We then harnessed the spatial nature of the Act model to examine the UCSP in more detail. We focused on the 2D and 3D settings (which are less artifical than the microchannel environment and allow cells to take on their preferred shapes), and investigated how the cell's migration mode changed when speed and persistence increased (Figure 3).

An important feature of the Act model is that it reproduces different cell shapes and migration modes (Niculescu et al., 2015). Low values of λ_{act} and max_{act} promote the formation of small and narrow protrusions that form and decay dynamically, giving rise to an amoeboid ("stop-and-go") migration mode (Figure 3A, left). By contrast, large values of λ_{act} and/or max_{act} favor the formation of broad, stable protrusions, yielding a more persistent "keratocyte-like" migration mode (Figure 3A, right).

Like with the microchannel data (Figure 2C), we again found a strong exponential correlation between speed and persistence when we stratified cells by max_{act} value (Figure 3B, Figure S2A in Supplementary Material). This time, however, the exponential increase in persistence was also accompanied by a transition from amoeboid to keratocyte-like cell shapes (insets in Figure 3B).

This transition between different migration modes is also visible in the distributions of the instantaneous speeds from our simulated cell tracks (Figure 3C, Figure S2B in Supplementary Material). The bimodal shape of this distribution – which is especially evident at low values of max_{act} – reflects the "stop-and-go" behavior of migrating Act cells: when the cell is in a "stop", it has a very low instantaneous speed of almost 0 pixels/MCS, whereas the "go" intervals of movement are responsible for the peak at a higher speed. Higher λ_{act} values not only increase migration speed (reflected by an upward shift of this second peak), but also reduce the amount

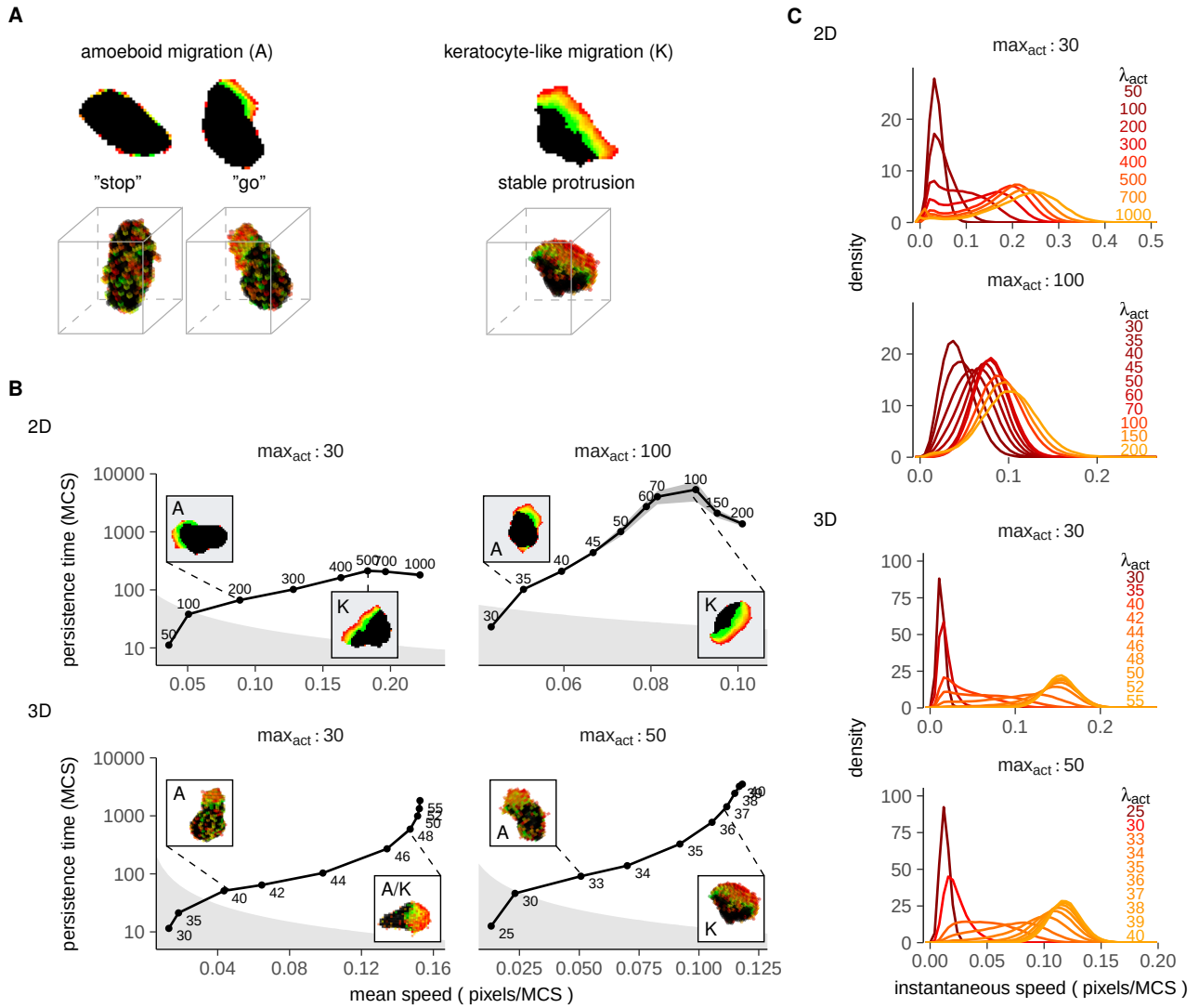

Figure 3: Speed-persistence coupling spans a range of migration modes. **(A)** Migration modes in the Act-model (see also (Niculescu et al., 2015)). Amoeboid cells are characterized by small, narrow protrusions that decay quickly and produce stop-and-go motion. Keratocyte-like cells are characterized by more stable, broad protrusions that do not decay easily. **(B)** Exponential speed-persistence coupling in 2D and 3D spans a transition form amoeboid to keratocyte-like motion. Plot shows mean ± SD of persistence time plotted against speed for different combinations of λ_{act} and max_{act}. Insets show representative cell shapes for the indicated parameters; shaded gray background indicates regions where the persistence time is lower than the time it takes for a cell to move 10% of its length. See also Figure S2A in Supplementary Material. **(C)** Distributions of the instantaneous speeds of 2D and 3D Act cells reveal a transition through different migration regimes. Cells go from not moving (single peak at speed ~0 pixels/MCS), via "stop-and-go" motility (bimodal distributions), to near-continuous movement (single peak at high speed). See also Figure S2B in Supplementary Material.

of time a cell spends in "stops" (reflected by a decrease in the size of the first peak). As stops provide an opportunity for the cell to change its direction (Figure 3A), the reduced "stopping time" at high λ_{act} values explains why Act cells with high λ_{act} values migrate not only faster, but also more persistently.

Together, these results demonstrate that the exponential speed-persistence coupling holds across different "regimes" of migration. At very low λ_{act}, the cell barely moves at all – as indicated by a single peak at instantaneous speeds of almost zero (Figure 3C). This corresponds to a cell without protrusions, spending most of its time in "stops". As λ_{act} increases, the cell enters a "stop-and-go", amoeboid migration regime (bimodal distributions), until finally it takes on a keratocite-like shape and almost never stops moving at the highest λ_{act} values.

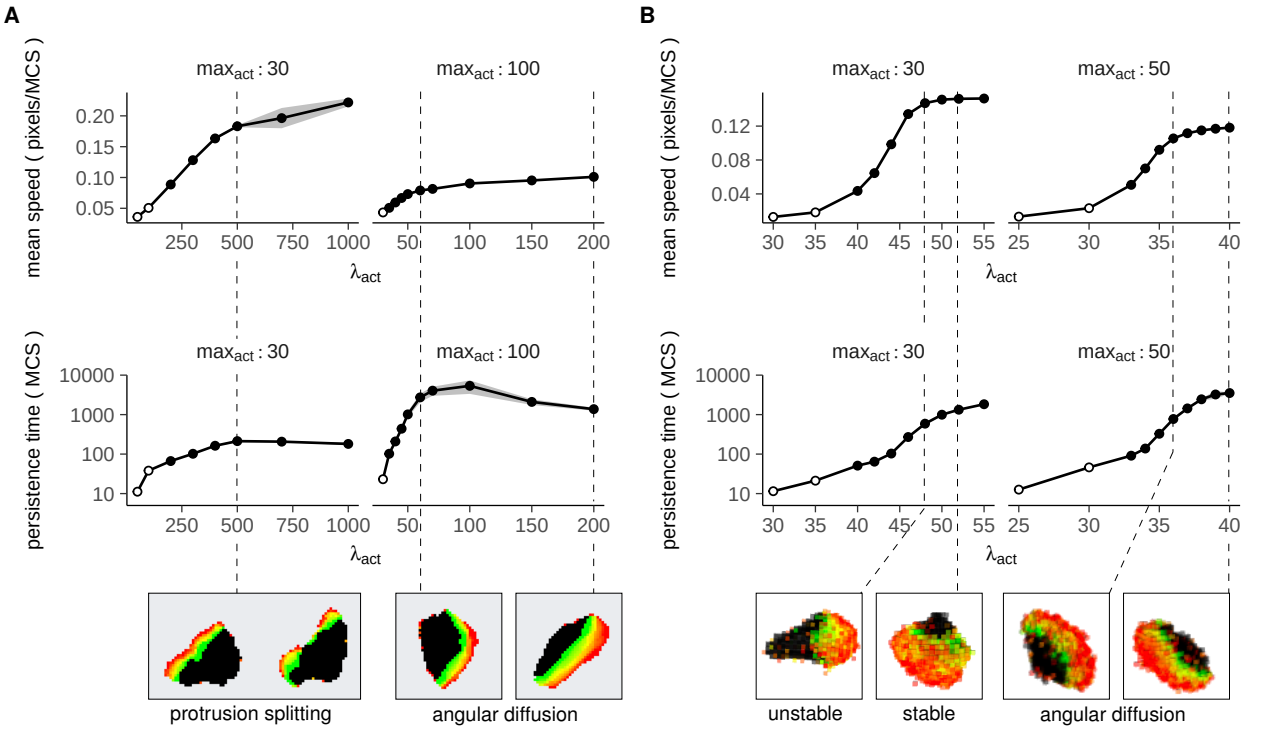

Figure 4: Cell shape dynamics limit both the speed and persistence of migrating cells. Mean ± SD of speed and persistence time of **(A)** 2D and **(B)** 3D Act cells, plotted against λ_{act} for different values of max_{act}. Open circles indicate points where the persistence time is lower than the time it takes the cell to move 10% of its length (corresponding to the points in the gray background in Figure 3B). Insets show cell shapes at the indicated parameter values.

2.4 Both Act cell speed and persistence saturate in a cell shape-dependent manner

Interestingly, our data also show the saturation of the persistence at higher cell speeds that was also reported in the experimental data (compare the 2D figures in Figure 3B to the data in (Maiuri et al., 2015)). In fact, this saturation was not limited to persistence. Whereas speed initially increased linearly with λ_{act}, it plateaued at higher λ_{act} values (Figure 4A,B, Figure S2C in Supplementary Material). The maximum speed reached depended on the protrusion shape-parameter max_{act}, but in all cases, the initial linear part of the graph spanned the entire transition from amoeboid to a keratocyte-like shape. This finding suggests that having to maintain a broad protrusion limits the speed a cell can reach. In line with this idea, we did not observe this saturation in microchannels, which prevent the cell from acquiring the broad protrusions observed in 2D and 3D (Figure S3A in Supplementary Material).

Similarly, the cell shape changes observed in 2D and 3D seem to put an upper bound on persistence that disappears when the cell is constrained by a microchannel (Figure 4A,B, Figure S2C, S3B in Supplementary Material). The initial exponential increase in persistence again spanned the entire transition from amoeboid to keratocyte protrusion shapes, before eventually saturating at a max_{act}-dependent value. Also this phenomenon seems to be linked to protrusion shapes. Whereas cells with low max_{act} do tend to form keratocyte-like protrusions at high λ_{act} values, these protrusions do not extend far into the cell and are prone to breaking – forcing the cell to turn towards one of the protrusion halves (Figure 4A). Although higher max_{act} values allow larger persistence times by letting broad protrusions extend farther into the cell and preventing them from breaking (Figure 4A,B), persistence still saturates eventually due to slight, stochastic turning within the general direction of the stable protrusion ("angular diffusion", Figure 4A,B) (Maiuri et al., 2015).

By showing how the shape of migrating cells puts a natural upper bound on both the speed and the persistence a cell can reach, these results explain the saturation of persistence observed by Maiuri et al (Maiuri et al., 2015). However, there was a striking effect of dimensionality on this process: although we observed shape-driven saturation in both 2D and 3D, the shape of the speed-persistence curve was different for 2D and

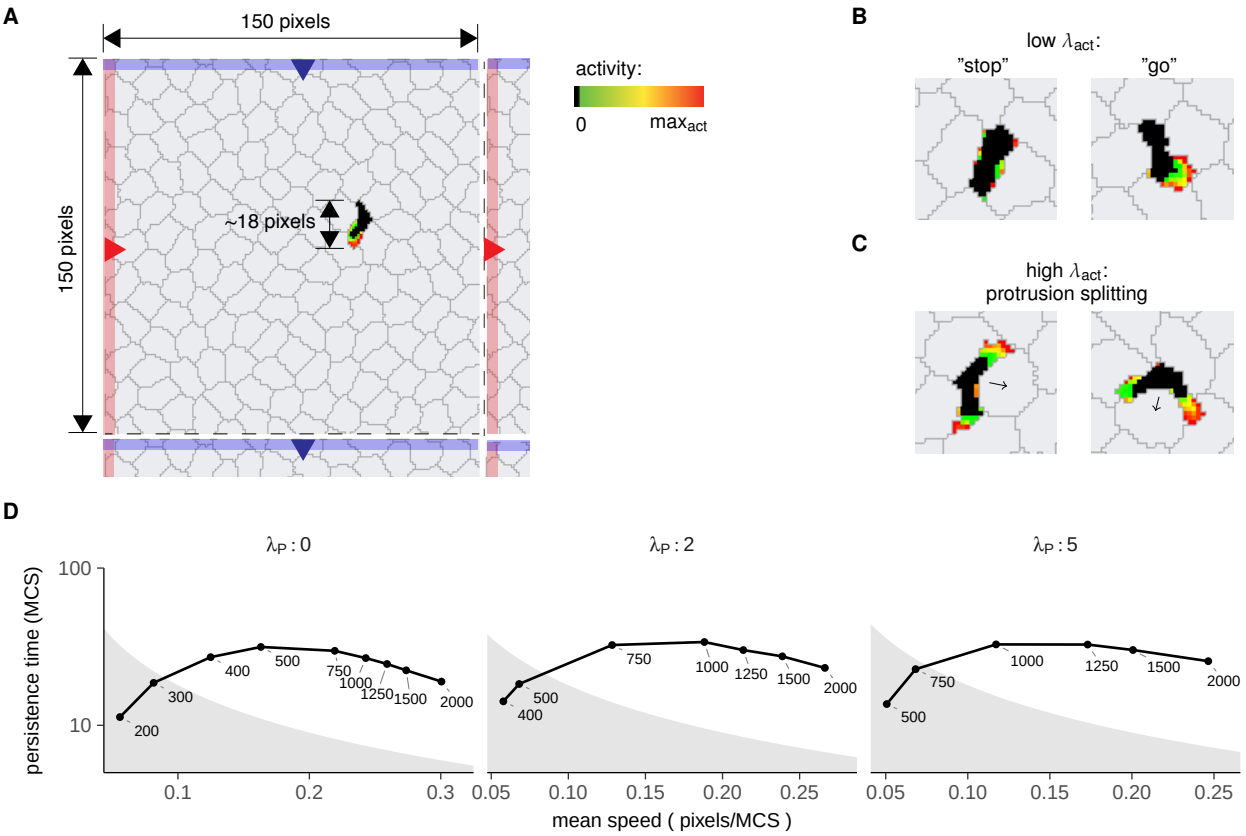

Figure 5: Environmental constraints limit T cell persistence in a model of the epidermis. **(A)** An Act T cell (black) moving in between keratinocytes (gray) in the epidermis. Simulations were performed in a 150 x 150 pixel grid with linked borders (for example, a cell moving off the grid towards the red region on the right re-enters the grid at the equivalent red region on the left). **(B,C)** Shapes of Act T cells constrained between keratinocytes. At lower λ_{act} values, T cells show typical amoeboid "stop-and-go" behavior. At higher λ_{act} values, cells do not obtain a broad, keratocyte-like shape, but stay elongated due to environmental constraints. At junctions between keratinocytes, however, protrusions tend to split. **(D)** Mean persistence time plotted against speed for different combinations of λ_{act} and the keratinocyte rigidity parameter λ_P (max_{act} = 20). Shaded gray background indicates regions where the persistence time is lower than the time it takes for a cell to move 10% of its length.

3D simulations (Figure 3B, 4). In both settings, speed and persistence saturated after an initial linear/exponential increase with λ_{act}. Yet, whereas persistence saturated before speed in 2D (Figure 4A), 3D Act cells showed a much stronger saturation of speed that preceded the saturation of persistence (Figure 4B). Thus, when both speed and persistence have a natural upper bound, the dominant saturation effect can be context-dependent – altering the shape of the speed-persistence curve.

2.5 Environmental constraints break the UCSP for T cell migration in the epidermis

After validating that the Act model robustly reproduces the UCSP, we applied this model to study our original question of how a crowded environment affects the speed and persistence of migrating T cells. Specifically, we modelled T cell migration in the epidermal layer of the skin. As one of the key entry points through which pathogens can enter the body, even healthy skin contains substantial numbers of T cells (Clark et al., 2006). T cells attracted to the epidermis during an infection can remain there for a long time: even a year after the resolution of an infection, specific T cells still persist in the same region of the epidermis (Gebhardt et al., 2009, 2011; Jiang et al., 2012; Zaid et al., 2014). Whereas subtle chemotaxis guides T cells towards infected cells during the effector phase (Ariotti et al., 2015), these remaining T cells actively patrol the epidermis without such chemotactic guidance (Ariotti et al., 2012) – migrating in patterns shaped by a combination of cell-intrinsic factors and environmental constraints. Importantly, even though the tight contacts between keratinocytes make the epidermis one of the most rigid environments T cells encounter *in vivo*, T cells in the epidermis are

nevertheless highly motile (Ariotti et al., 2012).

We therefore focused on this extreme example to examine how environmental structure can affect the UCSP. To this end, we simulated T cell migration in the skin as reported previously (Niculescu et al., 2015), placing an Act cell in a grid covered completely with keratinocytes (Figure 5A). Because of the opposing forces from the surrounding keratinocytes, cells now required higher λ_{act} forces to counter this resistance and start moving (Figure S4 in Supplementary Material). At sufficiently high λ_{act} values, they once again showed the characteristic "stop-and-go" motility before eventually switching to near-constant motion with hardly any stops (Figure 5B, Figure S4 in Supplementary Material).

Unlike Act cells in an unconstrained environment, these Act T cells did not switch from amoeboid to keratocyte-like cell shapes as λ_{act} increased. Cells at high λ_{act} now mostly maintained their amoeboid shape, probing their surroundings with narrow protrusions and migrating in the direction of their longest axis. However, when these cells approached a "T-junction" (Figure 5C), they sometimes formed a broad protrusion in the space between the keratinocytes that eventually split up into two separate protrusions going in opposite directions. This protrusion splitting caused the cell to slow down until one of the two active regions gained the upper hand.

In this set-up, increases in λ_{act} were once again associated with a higher speed that gradually saturated at high λ_{act} values (Figure S5A in Supplementary Material), but persistence times now saturated much earlier, reaching a plateau at ~30 MCS (Figure S5B in Supplementary Material). With cell speeds around ~0.2 pixels/MCS, this corresponds to persistent movement over distances in the range of ~5-10 pixels – which is roughly the distance the T cell can travel before arriving at another junction (Figure 5A). Thus, the structure of the environment appears to be the limiting factor for T cell persistence in this scenario.

This rapid saturation of persistence overruled the UCSP for T cells migrating in the skin, abrogating the coupling of speed and persistence (Figure 5D). This result was independent of the rigidity of the surrounding keratinocytes: although a reduction in the keratinocyte rigidity parameter λ_P increased the speeds that T cells could reach (Figure S5A in Supplementary Material), it did not affect the maximum persistence time (Figure S5B in Supplementary Material) or the absence ofspeed-persistence coupling (Figure 5D). These results demonstrate that although the UCSP appears to be valid for all migrating cells, cell-intrinsic speed-persistence coupling may be obscured when environmental factors place additional, more stringent constraints on persistence.

3 Discussion

To date, the UCSP remains the only general law describing cell motility across the complete spectrum of migrating cell types. Given the incredible diversity of the mechanisms driving cell migration in different cell types, it is not straightforward that such a general law should exist at all. Nevertheless, the UCSP is now firmly established: after its initial discovery (Maiuri et al., 2012), Wu et al later confirmed the UCSP in an independent study (Wu et al., 2014), and Maiuri et al explained it by showing that actin retrograde flow can mechanistically couple cell polarity to migration speed (Maiuri et al., 2015). Here, we again confirm this fundamental law of cell migration in an independent model and show – for the first time – how it relates to cell shape dynamics and environmental constraints.

The mathematical model of the UCSP described by Maiuri et al differs from the Act model in the level of detail used to describe cell polarity and cell shape. The Maiuri model treats the cell as a line along its length axis – describing describes both polarity molecule concentrations and actin retrograde flow only in this one dimension – and lacks a more detailed description of the cell shape and shape dynamics. By contrast, the Act model does reproduce realistic cell shapes and shape dynamics (Niculescu et al., 2015). Although it lacks an explicit description of the actin retrograde flow, it nevertheless reproduces the exponential speed-persistence coupling observed in the Maiuri model and in experimental data. Similar to the experimental data, this association is weak in heterogeneous cell populations – but becomes stronger when cells are stratified into more similar groups (in this case, by max_{act} value) (Figure 2B,C, 3B).

Because the Act model provides a more detailed description of cell shape than the Maiuri model, it allowed us to investigate how the UCSP interacts with cell shape dynamics. Firstly, our data show that speed-persistence coupling spans a transition between different cell shapes and migration modes (Figure 3). This finding highlights that cell shape and cell motility characteristics interact – consistent with several other studies showing a link between cell shape and speed within individual cell types (Keren et al., 2008; Ofer et al., 2011; Tweedy et al., 2013). Secondly, the model demonstrates that cell shape puts an upper bound on migratory speed and persistence: both saturated at high λ_{act} levels where the cell had attained a broader, more keratocyte-like shape (Figure 4). Interestingly, a similar shape-speed correlation with saturation at broad cell shapes was found in fish keratocytes (Keren et al., 2008). These observations clearly show that not only persistence, but also cell speed has a natural upper bound determined at least partly by cell shape dynamics. We also show an important role for dimensionality in this process, as the saturation of speed and persistence behaved differently in 2D versus 3D. Together, these results shed new light on the saturation of persistence observed in the experimental data: whereas persistence saturated before speed in all experimental settings considered by Maiuri et al (Maiuri et al., 2015), our model suggests that – depending on the cell's shape – scenarios in which speed saturates earlier could likewise exist.

In our *in silico* model of T cell migration in the epidermis, environmental constraints posed by the dense keratinocyte layer restricted persistent movement and obscured the UCSP (Figure 5) – showing that environmental constraints can overrule the UCSP in at least some of the environments T cells face *in vivo*. We therefore predict that speed-persistence coupling should not be visible in *in vivo* imaging data of T cells patrolling the epidermis: in such an environment, both speed and persistence likely reflect the maximum of what is feasible given the environmental constraints rather than being the result of an intrinsic coupling.

It is worth noting here that the epidermis is an extreme example of a confining environment, and that other tissues likely place less stringent constraints on T cell movement. This would allow a more important role for the UCSP in determining persistence in such tissues. Interestingly, thymocytes navigating the thymic cortex during positive selection perform a random walk at a low speed – whereas the same region also contains a population of cells with much higher speed and persistence, representing the cells that have already completed positive selection (Witt et al., 2005; Halkias et al., 2013). This finding shows that the slow-moving population of thymocytes still undergoing positive selection has not yet reached the maximal speed and persistence permitted by the environment – suggesting a role for the UCSP in this context. Future studies should elucidate whether the UCSP indeed applies in cortical thymocytes.

Our results have implications for studies investigating the efficiency of T cell search behavior. Motility characteristics such as speed and persistence are not independent parameters that can be tuned to generate "optimal" search behavior, but rather reflect a complex interplay between cell-intrinsic rules such as the UCSP and the topology of the environment. Random walk models of T cell search strategies should therefore consider that speed and persistence are subject to both cell-instrinsic and environmental constraints. As different models can often explain the same data, understanding these constraints will be crucial to select those models that are not only consistent with data, but represent search strategies that T cells might actually adopt *in vivo*.

4 Materials and Methods

4.1 Act model

For our simulations, we used the Act model as described in (Niculescu et al., 2015). Our JavaScript implementation of this model is available at http://github.com/jtextor/cpm.

Briefly, the Act model is an extension of the Cellular Potts Model that represents cells as collections of pixels on a 2D or 3D grid. These pixels randomly try to copy their cell's identity into neighbor pixels belonging to other cells. The probability that such a copy attempt will succeed depends on the global energy or Hamiltonian of the system, which is in turn determined by cell-cell adhesion and constraints on the cell's volume and perimeter. The success probability of a copy attempt therefore not only depends on the cell's shape, but also on that of the cell that it tries to copy into. Time in the CPM is measured in Monte Carlo Steps (MCS), where one MCS contains a number of copy attempts equal to the total number of pixels in the grid.

The Act model extends the CPM with positive feedback, such that pixels that were recently added to a cell (= recent "protrusive" activity) remember this activity for a period of $\max_{act}$ MCS – during which they become more likely to protrude again. This is accomplished via a negative contribution ΔH_{act} to the Hamiltonian for all copy attempts from a source pixel s in an active region into a target pixel t in a less active region:

$$\Delta H_{act}(s \to t) = -\frac{\lambda_{act}}{\max_{act}}(\mathrm{GM}_{act}(s) - \mathrm{GM}_{act}(t)) \quad (1)$$

where $\mathrm{GM}_{act}(p)$ of pixel p is the geometric mean of the activity values of all pixels in the (Moore) neighborhood of p. Thus, ΔH_{act} is negative when $\mathrm{GM}_{act}(s) > \mathrm{GM}_{act}(t)$.

For a complete description of the CPM, see (Niculescu et al., 2015). For details on parameters used, see section 4.2 below.

4.2 Simulations

Before the start of each simulation, cells were seeded in the middle of the grid and allowed a burnin time of 500 MCS to gain their optimal volume and shape. Every cell centroid was then tracked for a period of 50,000 MCS. To maximize measurement resolution while still allowing the cells to displace enough for an accurate determination of movement direction, cell centroids were recorded every 5 MCS.

4.2.1 Basic CPM parameters

For each experiment, we selected parameters combinations where cells had realistic shapes and migration behavior (see Table 1). Temperature, volume, perimeter, adhesion, and λ_V/λ_P were chosen such that cells stayed connected even at high $\max_{act}$ and λ_{act} values tested ("connectedness" at least 95% for at least 95% of the time for all simulations except skin simulations. See section "Connectedness" below). Except for $\max_{act}$ and λ_{act}, parameters were held constant within each experiment. Parameters for 1D and 2D simulations were mostly equal – except for the larger perimeter in 1D to account for the elongated shape of cells in microchannels. For 3D simulations, however, we had to select other parameters to account for changes in surface to volume ratio and thus altered relative contributions of the different terms to the total ΔH.

4.2.2 Act model parameters

To investigate the link between speed and persistence, we analyzed cell tracks with increasing λ_{act} while keeping $\max_{act}$ fixed (Table 2). Max_{act} values were chosen to obtain a range of protrusion sizes, from small protrusions to large protrusions occupying most – but not all – of the cell volume (see percentage active pixels analysis below). For each $\max_{act}$, a range of λ_{act} values was then chosen such that cells went from completely brownian motion (persistence time ~ 5 MCS, the time between subsequent measurements of cell location) to maximally persistent motion (persistence time ~ 10,000 MCS). Persistence times higher than 10,000 MCS were not considered, as such

Table 1: CPM parameters used in different experiments. Within each experiment, parameters were kept constant. Skin simulation parameters apply to the T cells; bracketed parameters indicate values used for the keratinocytes.

	1D	2D	3D	Skin
Grid size (pixels)	50000 x 12	10000 x 10000	1024 x 1024 x 1024	150 x 150
Linked grid borders	no	no	no	yes
Simulation duration (MCS)	50000	50000	50000	50000
Burnin time (MCS)	500	500	500	500
Temperature	20	20	7	20
Volume (pixels)	500	500	1800	100 (152)
λ_{Volume}	30	30	25	30 (30)
Perimeter	360	260	8600	130 (145)
$\lambda_{\text{Perimeter}}$	2	2	0.01	2 (0/2/5)
Adhesion cell-channel	15	-	-	-
Adhesion cell-ECM	20	20	5	20 (20)
Adhesion cell-cell	100	100	15	20 (20)
Adhesion T cell-keratinocyte	-	-	-	100

Table 2: Combinations of max_{act} and λ_{act} used in different experiments. For each max_{act}, λ_{act} values were chosen such that cells went from no persistence to maximal persistence.

Experiment	max_{act}	λ_{act}
1D	30	100, 200, 600, 800, 1000, 1200, 1400
	40	60, 80, 100, 200, 400, 600
	50	50, 60, 70, 80, 90, 95, 100
	60	40, 45, 50, 55, 60, 65, 70
	80	25, 30, 35, 38, 40, 42, 45
	100	30, 32, 34, 36, 38, 40
2D	30	50, 100, 200, 300, 400, 500, 700, 1000
	40	50, 75, 100, 150, 200, 250, 300, 500, 800, 1000
	50	50, 75, 100, 125, 150, 200, 300, 500
	60	40, 60, 80, 100, 120, 150, 250
	80	30, 40, 50, 60, 70, 100, 150, 200
	100	30, 35, 40, 45, 50, 60, 70, 100, 150, 200
3D	30	30, 35, 40, 42, 44, 46, 48, 50, 52, 55
	40	30, 35, 37, 38, 39, 40, 42, 45, 50
	50	25, 30, 33, 34, 35, 36, 37, 38, 39, 40

high persistences will likely be underestimated due to the finite total simulation time (50,000 MCS). For skin simulations, keratinocytes were modelled with $\text{max}_{\text{act}} = \lambda_{\text{act}} = 0$, and variable λ_{P}, T cells with $\text{max}_{\text{act}} = 20$ and variable λ_{act} (Table 3).

4.2.3 Microchannel simulations

To simulate migration of cells confined in a 1D microchannel, we created a 2D grid with a height of 10 pixels and a width of 50,000 pixels. Cells were confined by a layer of "barrier" pixels on the top and bottom of the grid, into which copy attempts were forbidden (yielding a total grid height of 12 pixels). Cells were seeded in the middle of the channel for each simulation.

Table 3: Combinations of keratinocyte λ_{P} and T cell λ_{act} used in the skin simulations.

Experiment	λ_{P}	λ_{act}
skin	0	200, 300, 400, 500, 750, 1000, 1250, 1500, 2000
	2	400, 500, 750, 1000, 1250, 1500, 2000
	5	500, 750, 1000, 1250, 1500, 2000

4.2.4 2D and 3D simulations

To simulate migration in 2D and 3D, we seeded single cells in the middle of an empty 2D (10,000 x 10,000 pixels) or 3D (1024 x 1024 x 1024 pixels) grid, respectively.

4.3 Analysis of cell shape and protrusions

During each simulation (every 5 MCS), we recorded not only the position of the cell's centroid, but also several other cell properties to keep track of the cell's shape and degree of polarization (see below).

4.3.1 Connectedness

In the CPM, the pixels belonging to a single cell are held together mostly via the adhesion term in the Hamiltonian, which favours cell shapes where pixels belonging to the same cell adhere to each other. However, this adhesive force can become negligible relative to the other ΔH terms – for example when ΔH_{act} is large due to a high λ_{act}. Thus – especially in 3D – cells may break apart at high values of λ_{act}, despite the unfavourable changes in adhesion energy associated with this break.

As frequent cell breaking causes artefacts in the tracking data that may bias the measurement of speed and persistence, it is important to use parameter ranges that prevent such an unbalanced contribution of the different ΔH terms. To estimate the frequency of cell breaking, we therefore recorded the *connectedness* (C) of the cell every 5 MCS of each simulation.

C represents the probability that two randomly chosen pixels from the same cell are part of a single, unbroken unit. To compute C_i of a cell i, we represent the cell i as a graph G_i where every node p is a pixel belonging to cell i, and pixels are connected by an edge if they are adjacent to each other on the CPM grid (that is, if they are from the same Moore neighborhood). We then group the pixels into n *connected components* $[c_1, ..., c_n]$ – that is, groups of pixels where for every pair of pixels ($p_1 \in c, p_2 \in c$), it is possible to walk from p_1 to p_2 via the edges of graph G_i. We then define C_i as:

$$C_i = \sum_{k=1}^{n} \left(\frac{V_k}{V_i} \right)^2 \tag{2}$$

where V_k is the pixel volume of connected component c_k in G_i, and V_i the total volume of cell i. Thus, an unbroken cell – which by definition has only one connected component – has $C_i = 1$, whereas a cell broken into many isolated pixels has $C_i \to 0$.

4.3.2 Percentage active pixels

As a measure of the size of the active protrusion of a cell, we counted the percentage of pixels of that cell with an Act-model activity > 0.

4.4 Track analysis

All simulated cell tracks were analyzed in R (version 3.4.3) using the MotilityLab package (version 0.2.5). To compute speed and persistence, we performed step-based analyses on 4 groups of 5 simulated tracks (see below), yielding 4 estimates of speed and persistence for every parameter combination. These four values were then used to estimate the overall value (mean) and measurement precision (standard deviation) of speed and persistence at that parameter combination.

4.4.1 Speed

To compute speeds, we first computed instantaneous speeds at every step in every cell track (using the "speed" function of MotilityLab). The reported mean speed was then the average of all the instantaneous speeds in the recorded tracks.

4.4.2 Persistence

To measure the persistence of a moving cell, consider the vectors $\vec{v}_{(t)}$ (movement direction at time t) and $\vec{v}_{(t+\Delta t)}$ (movement direction at time $t + \Delta t$). When the cell moves persistently, we expect that the direction of movement at $t + \Delta t$ is similar to that at t, even for relatively large values of Δt. By contrast, for a cell undergoing random Brownian motion, the direction of $\vec{v}_{(t+\Delta t)}$ is probably unrelated to that of $\vec{v}_{(t)}$.

To quantify this, consider the dot product between the movement vectors $\vec{v}_t$ and $\vec{v}_{t+\Delta t}$:

$$\vec{v}_{(t)} \cdot \vec{v}_{(t+\Delta t)} \stackrel{\text{def}}{=} ||\vec{v}_{(t)}||||\vec{v}_{(t+\Delta t)}|| \cos\theta \tag{3}$$

Here, $\cos\theta$ of the angle between vectors $\vec{v}_{(t)}$ and $\vec{v}_{(t+\Delta t)}$ is 1 when the vectors align perfectly ($\theta = 0$) , -1 when they are exactly opposite ($\theta = 180$), and somewhere in between for all other angles. When we take $\Delta t = 0$, equation 3 simplifies to:

$$\vec{v}_{(t)} \cdot \vec{v}_{(t+\Delta t)} = \vec{v}_{(t)} \cdot \vec{v}_{(t)} = ||\vec{v}_{(t)}||||\vec{v}_{(t)}|| \cos 0 = ||\vec{v}_{(t)}||^2 \tag{4}$$

As $||\vec{v}_{(t)}||$ equals the instantaneous speed at time t, the average of this dot product for different values of t with $\Delta t = 0$ is just the squared mean speed $\bar{v}^2$.

However, when we increase Δt, the vectors $\vec{v}_{(t)}$ and $\vec{v}_{(t+\Delta t)}$ are no longer perfectly aligned, and their dot product becomes smaller. The rate at which this decay occurs depends on the motility mode of a cell: for a given Δt, persistent cells will on average have a smaller θ and thus a larger dot product than cells undergoing Brownian motion. Thus, to compute persistence, we first construct the *autocovariance curve* of the average dot product $\vec{v}_{(t)} \cdot \vec{v}_{(t+\Delta t)}$ as a function of Δt (using the "overallDot" function of the MotilityLab package). As a measure of persistence, we then compute the half-life τ of this autocovariance curve for which:

$$\frac{\vec{v}_{(t)} \cdot \vec{v}_{(t+\tau)}}{\vec{v}_{(t)} \cdot \vec{v}_{(t+0)}} = \frac{||\vec{v}_{(t)}||||\vec{v}_{(t+\tau)}|| \cos\theta}{||\vec{v}_{(t)}||^2} = 0.5 \tag{5}$$

As the dot product decays more slowly for more persistent cells, high values of τ indicate persistent movement. Note that, as the *average* $||\vec{v}_{(t)}||||\vec{v}_{(t+\tau)}|| = ||\vec{v}_{(t)}||^2 = \bar{v}^2$, τ is independent of the mean speed $\bar{v}$, even though the dot product is not.

Conflict of Interest Statement

The authors declare that the research was conducted in the absence of any commercial or financial relationships that could be construed as a potential conflict of interest.

Author Contributions

IW, IN, NG, RdB, and JT designed the research. IW, IN, and MK performed simulations and analyzed the data. IW and JT wrote the paper; NG and RB critically revised the manuscript.

Funding

IW was supported by a Radboudumc PhD grant. JT was supported by a Young Investigator Grant (10620) from KWF Kankerbestrijding.

References

Ariotti, S., Beltman, J. B., Borsje, R., Hoekstra, M. E., Halford, W. P., Haanen, J. B. A. G., et al. (2015). Subtle CXCR3-Dependent Chemotaxis of CTLs within Infected Tissue Allows Efficient Target Localization. *The Journal of Immunology* 195, 5285–5295. doi:10.4049/jimmunol.1500853

Ariotti, S., Beltman, J. B., Chodaczek, G., Hoekstra, M. E., Beek, A. E. v., Gomez-Eerland, R., et al. (2012). Tissue-resident memory CD8+ T cells continuously patrol skin epithelia to quickly recognize local antigen. *Proceedings of the National Academy of Sciences* 109, 19739–19744. doi:10.1073/pnas.1208927109

Bajnoff, M., Egen, J. G., Koo, L. Y., Laugier, J. P., Brau, F., Glaichenhaus, N., et al. (2006). Stromal Cell Networks Regulate Lymphocyte Entry, Migration, and Territoriality in Lymph Nodes. *Immunity* 25, 989–1001. doi:10.1016/j.immuni.2006.10.011

Beauchemin, C., Dixit, N. M., and Perelson, A. S. (2007). Characterizing T Cell Movement within Lymph Nodes in the Absence of Antigen. *The Journal of Immunology* 178, 5505–5512. doi:10.4049/jimmunol.178.9.5505

Beltman, J. B., Mare, A. F. M., Lynch, J. N., Miller, M. J., and Boer, R. J. d. (2007). Lymph node topology dictates T cell migration behavior. *Journal of Experimental Medicine* 204, 771–780. doi:10.1084/jem.20061278

Borgne, M. L., Ladi, E., Dzhagalov, I., Herzmark, P., Liao, Y. F., Chakraborty, A. K., et al. (2009). The impact of negative selection on thymocyte migration in the medulla. *Nature Immunology* 10, 823–830. doi:10.1038/ni.1761

Bnichou, O., Loverdo, C., Moreau, M., and Voituriez, R. (2011). Intermittent search strategies. *Reviews of Modern Physics* 83, 81–129. doi:10.1103/RevModPhys.83.81

Chupeau, M., Bnichou, O., and Voituriez, R. (2015). Cover times of random searches. *Nature Physics* 11, 844–847. doi:10.1038/nphys3413

Clark, R. A., Chong, B., Mirchandani, N., Brinster, N. K., Yamanaka, K.-i., Dowgiert, R. K., et al. (2006). The Vast Majority of CLA+ T Cells Are Resident in Normal Skin. *The Journal of Immunology* 176, 4431–4439. doi:10.4049/jimmunol.176.7.4431

Gebhardt, T., Wakim, L. M., Eidsmo, L., Reading, P. C., Heath, W. R., and Carbone, F. R. (2009). Memory T cells in nonlymphoid tissue that provide enhanced local immunity during infection with herpes simplex virus. *Nature Immunology* 10, 524–530. doi:10.1038/ni.1718

Gebhardt, T., Whitney, P. G., Zaid, A., Mackay, L. K., Brooks, A. G., Heath, W. R., et al. (2011). Different patterns of peripheral migration by memory $CD4^+$ and $CD8^+$ T cells. *Nature* 477, 216–219. doi:10.1038/nature10339

Germain, R. N., Robey, E. A., and Cahalan, M. D. (2012). A Decade of Imaging Cellular Motility and Interaction Dynamics in the Immune System. *Science* 336, 1676–1681. doi:10.1126/science.1221063

Halkias, J., Melichar, H. J., Taylor, K. T., Ross, J. O., Yen, B., Cooper, S. B., et al. (2013). Opposing chemokine gradients control human thymocyte migration in situ. *The Journal of Clinical Investigation* 123, 2131–2142. doi:10.1172/JCI67175

Jiang, X., Clark, R. A., Liu, L., Wagers, A. J., Fuhlbrigge, R. C., and Kupper, T. S. (2012). Skin infection generates non-migratory memory $CD8^+$ T_{rm} cells providing global skin immunity. *Nature* 483, 227–231. doi:10.1038/nature10851

Keren, K., Pincus, Z., Allen, G. M., Barnhart, E. L., Marriott, G., Mogilner, A., et al. (2008). Mechanism of shape determination in motile cells. *Nature* 453, 475–480. doi:10.1038/nature06952

Klein, L. (2009). Dead man walking: how thymocytes scan the medulla. *Nature Immunology* 10, 809–811. doi:10.1038/ni0809-809

Krummel, M. F., Bartumeus, F., and Grard, A. (2016). T cell migration, search strategies and mechanisms. *Nature Reviews Immunology* 16, 193–201. doi:10.1038/nri.2015.16

Maiuri, P., Rupprecht, J.-F., Wieser, S., Ruprecht, V., Bnichou, O., Carpi, N., et al. (2015). Actin Flows Mediate a Universal Coupling between Cell Speed and Cell Persistence: Cell 161, 374–386. doi:https://doi.org/10.1016/j.cell.2015.01.056

Maiuri, P., Terriac, E., Paul-Gilloteaux, P., Vignaud, T., McNally, K., Onuffer, J., et al. (2012). The first World Cell Race. *Current Biology* 22, R673–R675. doi:10.1016/j.cub.2012.07.052

Miller, M. J., Wei, S. H., Cahalan, M. D., and Parker, I. (2003). Autonomous T cell trafficking examined in vivo with intravital two-photon microscopy. *Proceedings of the National Academy of Sciences* 100, 2604–2609. doi:10.1073/pnas.2628040100

Miller, M. J., Wei, S. H., Parker, I., and Cahalan, M. D. (2002). Two-Photon Imaging of Lymphocyte Motility and Antigen Response in Intact Lymph Node. *Science* 296, 1869–1873. doi:10.1126/science.1070051

Niculescu, I., Textor, J., and de Boer, R. J. (2015). Crawling and Gliding: A Computational Model for Shape-Driven Cell Migration. *PLOS Computational Biology* 11, 1–22. doi:10.1371/journal.pcbi.1004280

Ofer, N., Mogilner, A., and Keren, K. (2011). Actin disassembly clock determines shape and speed of lamellipodial fragments. *Proceedings of the National Academy of Sciences* 108, 20394–20399. doi:10.1073/pnas.1105333108

Tejedor, V., Voituriez, R., and Bnichou, O. (2012). Optimizing Persistent Random Searches. *Physical Review Letters* 108, 088103. doi:10.1103/PhysRevLett.108.088103

Tweedy, L., Meier, B., Stephan, J., Heinrich, D., and Endres, R. G. (2013). Distinct cell shapes determine accurate chemotaxis. *Scientific Reports* 3, 2606. doi:10.1038/srep02606

Witt, C. M., Raychaudhuri, S., Schaefer, B., Chakraborty, A. K., and Robey, E. A. (2005). Directed Migration of Positively Selected Thymocytes Visualized in Real Time. *PLOS Biology* 3, e160. doi:10.1371/journal.pbio.0030160

Wu, P.-H., Giri, A., Sun, S. X., and Wirtz, D. (2014). Three-dimensional cell migration does not follow a random walk. *Proceedings of the National Academy of Sciences* 111, 3949–3954. doi:10.1073/pnas.1318967111

Zaid, A., Mackay, L. K., Rahimpour, A., Braun, A., Veldhoen, M., Carbone, F. R., et al. (2014). Persistence of skin-resident memory T cells within an epidermal niche. *Proceedings of the National Academy of Sciences* 111, 5307–5312. doi:10.1073/pnas.1322292111

Supplementary Figures

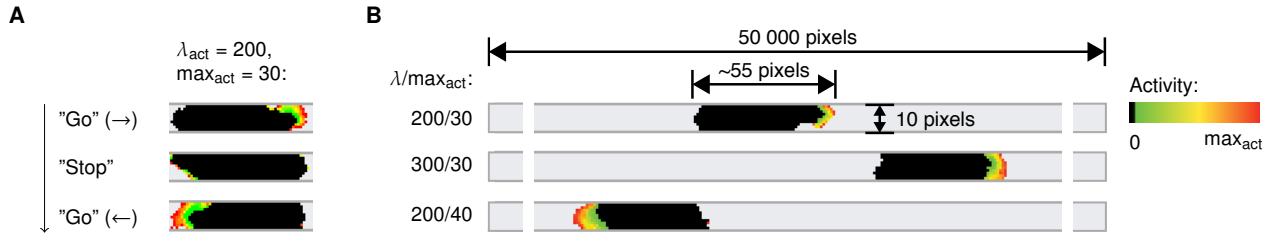

Figure S1: Act cells in microchannels have "stop-and-go" motility and variable protrusion sizes. **(A)** Example of "stop-and-go" motility. When a protrusion decays, the cell stops until a new protrusion forms – which may be in another direction. **(B)** Example cells for different combinations of the parameters max_{act}/ λ_{act}.

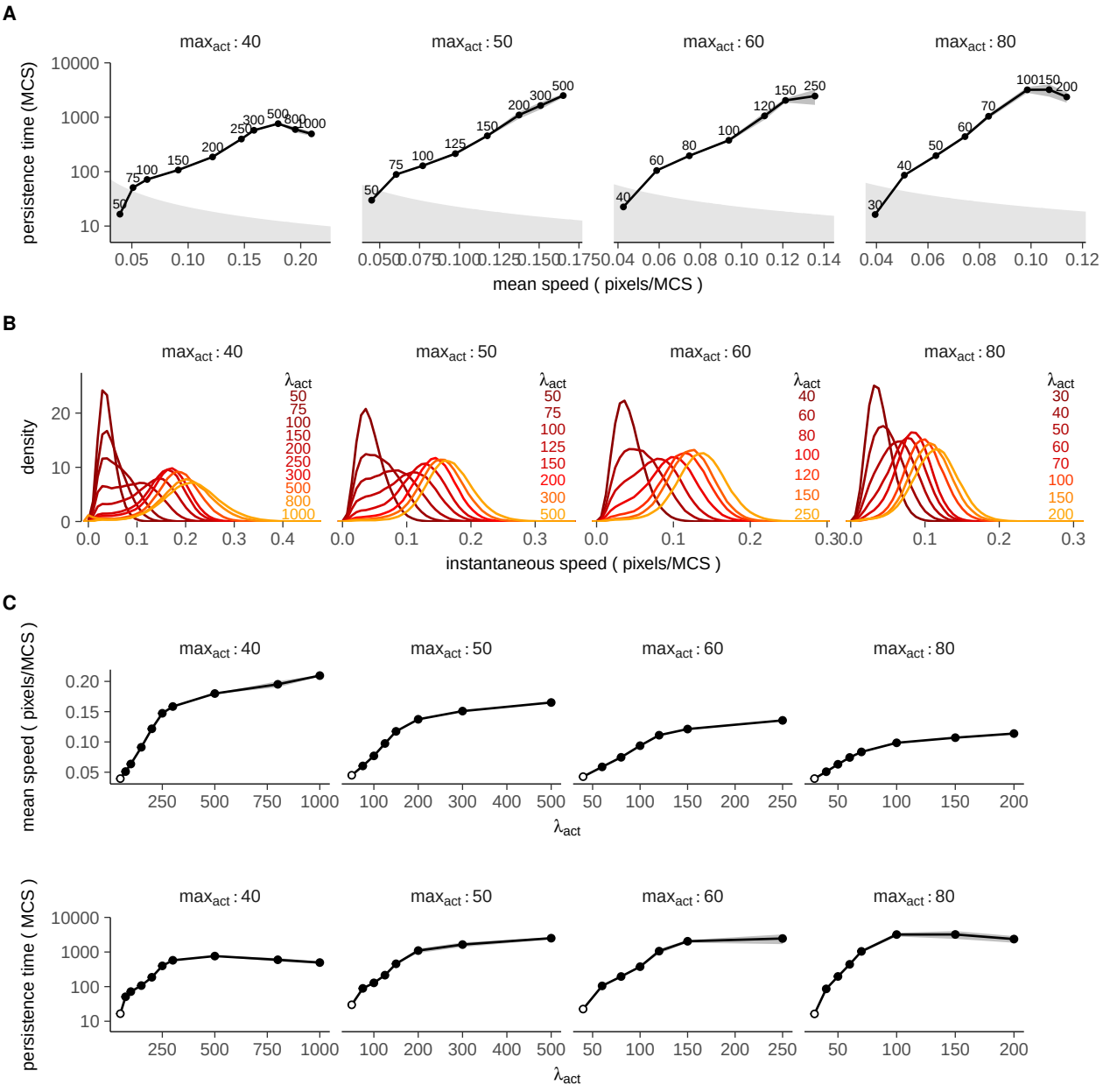

Figure S2: Act cells in 2D show similar behavior for different values of max_{act}, see also Figure 3B,C and 4A. Plots show **(A)** Exponential speed-persistence coupling, **(B)** Distributions of instantaneous speeds, and **(C)** Saturation of speed and persistence at high λ_{act} values.

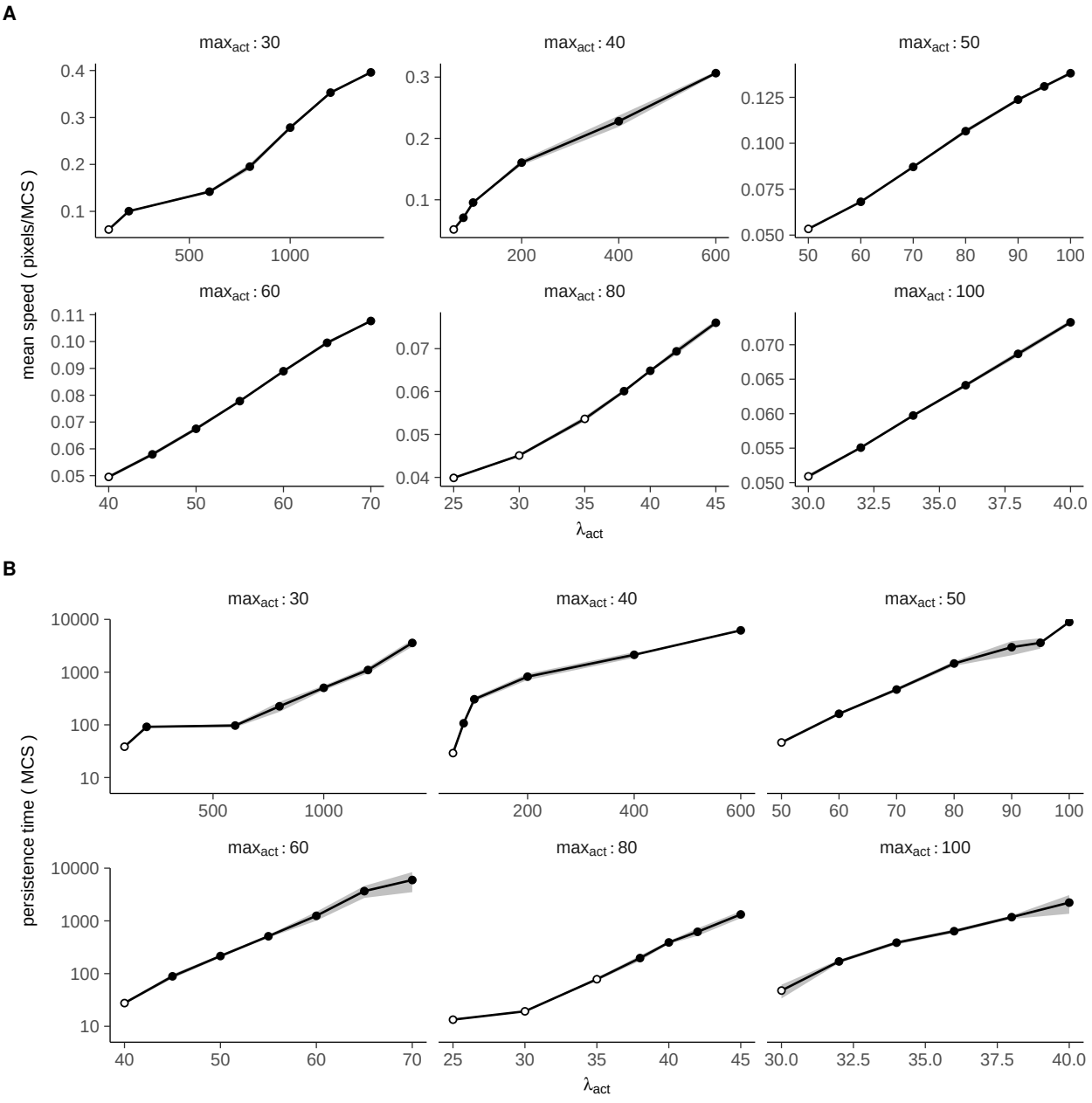

Figure S3: Confinement of Act cells in microchannels slows down saturation of speed and persistence. Plots show mean ± SD of **(A)** cell speed, and **(B)** persistence as a function of λ_{act}, for different values of max_{act}. Open circles indicate points where the persistence time is lower than the time it takes the cell to move 10% of its length (corresponding to points in the gray region in Figure 2).

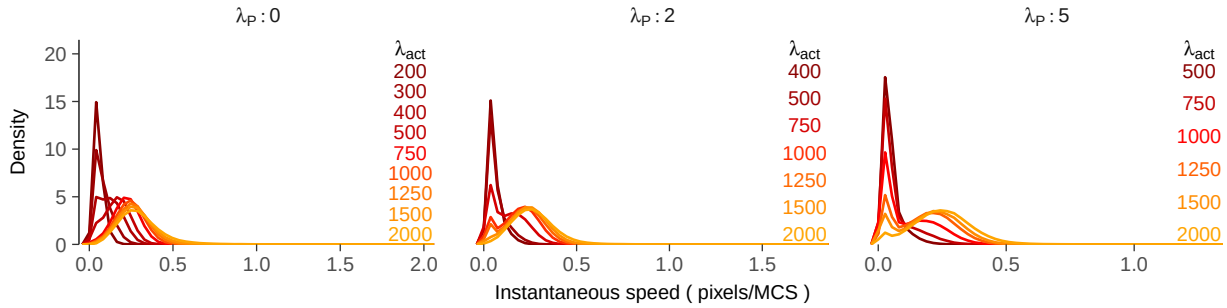

Figure S4: Act T cells in skin display ”stop-and-go” behavior. Plots show distributions of instantaneous speed for different values of the tissue rigidity parameter λ_P and migration parameter λ_{act} (see also Figures 3C and S2B).

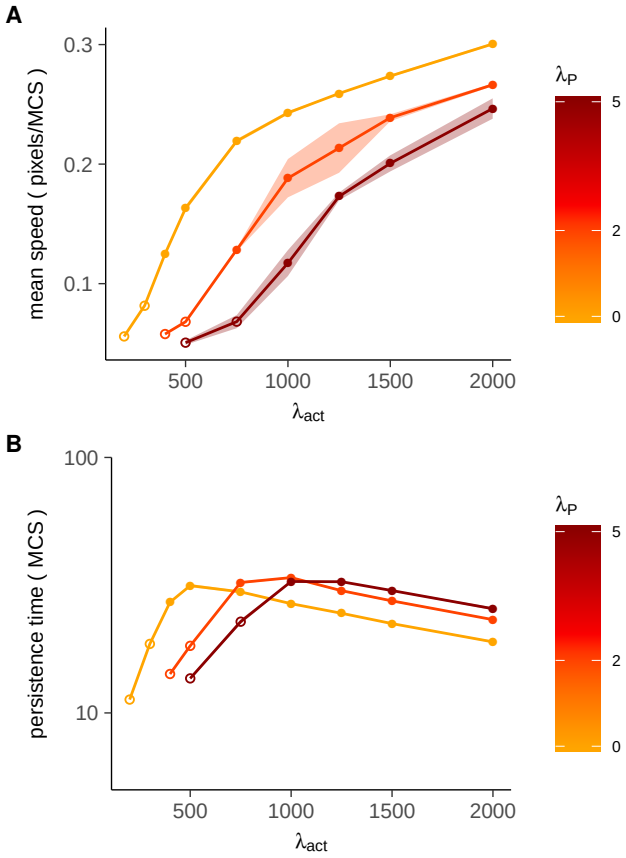

Figure S5: Both speed and persistence saturate for T cells moving in skin. Plots show mean ± SD of **(A)** cell speed, and **(B)** persistence as a function of λ_{act}, for different values of the tissue rigidity parameter λ_P. Open circles indicate points where the persistence time is lower than the time it takes the cell to move 10% of its length (corresponding to points in the gray region in Figure 5).